https://doi.org/10.1007/s41230-022-1230-z

Microstructure and mechanical properties of a low activation cast WTaHfTiZr refractory high-entropy alloy

Xian-neng Ma[1], Yi-fei Hu[1], **Kai Wang[2, 3], Hai-long Zhang[4], Zi-tian Fan[1], Jin-ping Suo[1], and *Xin-wang Liu[1]

1. State Key Laboratory of Materials Processing and Die & Mould Technology, School of Materials Science and Engineering, Huazhong University of Science and Technology, Wuhan 430074, China

2. Dekai Intelligent Casting Co., Ltd., Zhuozhou 072750, Hebei, China

3. China Iron and Steel Research Institute Group, Beijing 100081, China

4. AECC South Industry Company Limited, Zhuzhou 412002, Hunan, China

Abstract: In the face of the requirement that nuclear fusion reactor materials exhibit more excellent thermal, mechanical and physical properties, a novel refractory high-entropy alloy, WTaHfTiZr was proposed. The constituent elements were selected in consideration of low activation, high melting point and high thermostability. The alloys were prepared by arc melting. The as-cast alloy shows a dendrite microstructure with two disordered BCC phases, which caused by the preferential nucleation of W and Ta with much higher melting points during solidification. It exhibits a high compressive yield strength of 1,900 MPa and fracture strain of 8.1% at room temperature, and its yield strengths are up to 612 MPa at 700 °C and 203 MPa at 1,000 °C, respectively. The high strengths are attributed mainly to solid solution strengthening and second phase strengthening. This alloy shows great promise as one of the next-generation nuclear fusion reactor materials.

Keywords: refractory high-entropy alloy; phase structure; microstructure; mechanical properties

CLC numbers: TG146; **Document code:** A; **Article ID:** 1672-6421(2022)06-489-06

***Xin-wang Liu**

Male, born in 1982, Ph.D, Professor. His research interests mainly focus on as-cast microstructure refinement, strengthening and phase transformation of aluminum, titanium, and high-entropy alloys.

E-mail: liuxw@hust.edu.cn

****Kai Wang**

E-mail: wangkai483@aliyun.com

Received: 2021-12-15;
Accepted: 2022-02-23

1 Introduction

In a nuclear fusion reaction, the fusion materials come into close contact with high-temperature plasma and need to bear various transient and steady-state thermal loads [1]. Furthermore, nuclear fusion reactor materials are bombarded with high-energy neutrons over time, making them radioactive [2]. As a result, nuclear fusion reactor materials should have appropriate mechanical properties, low activation, and quick induced radioactive decay features [3].

At present, tungsten alloys, beryllium alloys, and carbon and its composite materials are the most commonly studied materials for nuclear fusion reactors [4-7]. However, these materials have various disadvantages such as high brittleness and irradiation embrittlement of tungsten [2, 6], low melting point, and toxic oxides of beryllium [8]. Carbon and its composite materials have insufficient strength and a short life [9]. Therefore, development of novel alloy systems with superior properties has become a major focus in this field.

High-entropy alloys (HEAs), proposed in 2004, have shown unique properties, such as high mechanical strength and hardness, excellent temper softening resistance, thermal stability, and good wear, oxidation, corrosion and creep resistance [10, 11]. Furthermore, refractory high-entropy alloys (RHEAs) mainly comprising refractory elements have been improved to develop novel heat-resistant alloys for aerospace field.

Senkov et al. [12] first proposed two equiatomic alloys, WTaNbMo and WTaNbMoV. Despite their remarkable high-temperature strength, these two RHEAs are brittle at room temperature. Therefore, researchers attempted to explore more RHEAs systems with excellent comprehensive properties. A series of RHEAs have been reported including MoNbHfZrTi, HfNbTaTiZrW, HfNbTaTiZrMoW, W_xTaTiVCr, HfMoTaTiZr, HfMoNbTaTiZr, and $Ti_2VNbMoZr_x$ [13–17]. Each of these RHEAs has a simple phase structure and excellent performance at high temperatures. Some RHEAs have a good thermal stability in terms of radiation damage resistance, owing to the composition complexity delaying the establishment of dislocation loops, reducing dislocation mobility, and promoting phase stability [18, 19]. However, these RHEAs contain high-activation elements, such as Mo, Nb, which cannot be used in nuclear fusion fields [13]. However, the unique high-temperature properties of these RHEAs reveal a high potential as nuclear fusion reactor materials after elaborate compositional design [20, 21]. There is currently a scarcity of research on RHEAs consisting of low-activated components, which can lessen the damage caused by irradiation materials while also being preserved and reused [22–24].

In this work, low activation elements W, Ta, Hf, Ti and Zr were selected to form an equiatomic WTaHfTiZr RHEA. Its phase constitution, microstructure and mechanical properties at room and elevated temperatures were investigated. The relevant mechanisms of phase formation and strengthening were also discussed.

2 Experimental procedure

WTaHfTiZr alloy buttons were prepared by arc-melting a mixture of pure metals (purity>99.9wt.%) in a high-purity argon atmosphere. After the raw materials were loaded in the arc melting furnace, the chamber was first evacuated to ~5×10^{-2} Pa and then backfilled with pure Ar and evacuated twice to dilute the residual air inside the chamber, finally backfilling a pressure of ~4×10^{4} Pa. Before the materials were melted, a small piece of pure Ti was melted to getter any residual air that might be present in the chamber. The buttons were remelted and flipped seven times to ensure chemical homogeneity.

The phase constitution and microstructure were investigated using X-ray diffraction (XRD) and scanning electron microscopy (SEM). The XRD analysis was performed using a SHIMADZU XRD-6100 X-ray diffractometer using Cu Kα radiation (λ=0.154 nm) with the range of 20°–100° at a speed of 5°·min^{-1}. The microstructure observation was conducted utilizing a Zeiss AURIGA FIB-SEM scanning electron microscope operated at the back-scatter electron (BSE) mode equipped with energy-dispersive X-ray spectroscopy (EDS) X-Max^N at an accelerating voltage of 20 kV. The room-temperature compressive properties were evaluated using an AG-IC 100 kN universal testing machine in the air. The elevated-temperature compressive properties were evaluated using a dynamic thermal simulation testing machine (Gleeble-3500). The strain rates are 10^{-3} s^{-1} at both room and high temperatures.

3 Results

3.1 Phase constitution and microstructure

The XRD pattern of as-cast WTaHfTiZr RHEA is shown in Fig. 1. The XRD spectrum reveals that the present alloy is composed of two BCC solid solution phases (denoted as BCC1 and BCC2). The Bragg angles corresponding to the peaks of BCC1 are lower than those of BCC2, which indicates that the lattice parameter of BCC1 is greater than BCC2. The lattice parameters of the BCC1 and BCC2 phases were calculated to be 0.343 nm and 0.326 nm, respectively.

Microstructures of the as-cast WTaHfTiZr RHEA are shown in Fig. 2. The microstructure in Fig. 2(a) indicates that the alloy has a dendritic feature. The chemical compositions of the interdendrite (IR) and dendrite (DR) regions were tested by SEM-EDS, the results of which are attached in the upper right of Fig. 2(a). W and Ta are enriched in dendrites, while the interdendrite region is rich in Hf, Ti and Zr. The enlarged interdendrite region in Fig. 2(b) reveals a mass of submicro precipitate particles which are enriched in W and Ta. The chemical composition of the interdendrite precipitates is similar to that of the dendrite arms. The EDS elemental maps of the WTaHfTiZr RHEA are shown in Fig. 3. The interdendrite region is enriched in light elements of Hf, Ti and Zr and the dendrite region is enriched with heavy elements of W and Ta, which are consistent with the element distributions in Fig. 2. Due to the fact that W and Ta have smaller atomic radii (0.137 nm and 0.143 nm) than those of the other three elements Ti, Zr, and Hf (0.146 nm, 0.160 nm and 0.158 nm) [10], the interdendrites rich in Ti, Zr, and Hf correspond to the BCC1 phase, while the dendrites and interdendritic particles rich in W and Ta are BCC2 phase.

According to the SEM-EDS chemical compositions of different regions in the dendritic structures, the segregation degree was calculated, which was expressed by the segregation ratio (K) [14]:

$$K = \frac{(C_{\mathrm{DR}})_i}{(C_{\mathrm{ID}})_i} \tag{1}$$

where $(C_{\mathrm{DR}})_i$ and $(C_{\mathrm{ID}})_i$ are the atomic percentage of element i in dendrite and interdendrite regions, respectively. The greater the difference between K and 1 (no segregation), the more serious

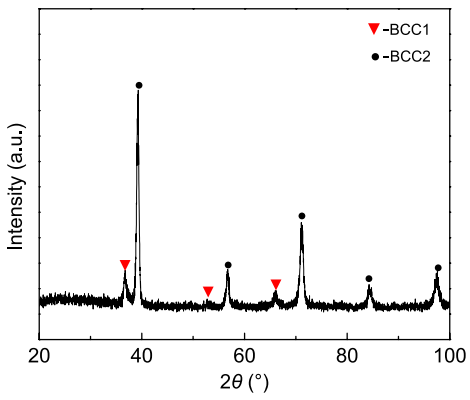

Fig. 1: XRD pattern of as-cast WTaHfTiZr RHEA

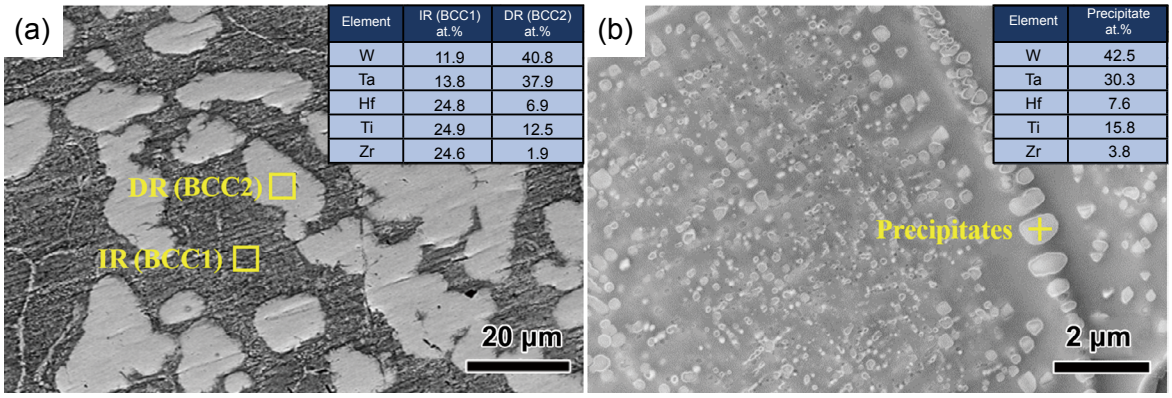

Fig. 2: SEM-BSE micrograph of as-cast WTaHfTiZr RHEA (a) and enlarged microstructure of the interdendritic region (b). SEM-EDS results of dendrite, interdendrite (a) and precipitates in the interdendritic region (b) are attached in the upper right corners

the segregation. Segregations of all elements in this RHEA are listed in Table 1. The elements in the WTaHfTiZr alloy have a serious segregation, which can also be clearly seen in Fig. 3.

3.2 Mechanical properties

Figure 4(a) shows compressive stress-strain curves of the cast WTaHfTiZr RHEA at different temperatures. The mechanical properties including yield strength, compressive strength and fracture strain are extracted from the compressive curves and presented in Table 2. The room-temperature yield strength and compressive strength are 1,900 MPa and 2,343 MPa, respectively, and the fracture strain is about 8.1%. At elevated temperatures, the alloy shows attractive yield strengths of 612 MPa and 203 MPa at 700 °C and 1,000 °C, respectively, and no fracture occurs up to strains of 40%.

Table 1: Chemical compositions in dendrite and interdendritic regions of as-cast WTaHfTiZr alloy and the calculated segregation ratio (*K*)

	W	Ta	Hf	Ti	Zr
Dendrite (at.%)	40.8	37.9	6.9	12.5	1.9
Interdendrite (at.%)	11.9	13.8	24.8	24.9	24.6
K	3.43	2.75	0.28	0.50	0.08

Figure 4(b) shows the comparison of compressive yield strength between the WTaHfTiZr RHEA and W and some low activation multicomponent alloys that shows promise for fusion reactor applications obtained from references [25-28]. It can be found that the WTaHfTiZr RHEA has a superior compressive yield strength to most compared low activation alloys at room temperature and 1,000 °C. In intermediate temperature ranges, the yield strength of the WTaHfTiZr RHEA is lower than that of some low activation alloys, especially $VCrFeTa_{0.2}W_{0.2}$. However, the $VCrFeTa_{0.2}W_{0.2}$ HEA is not in the as-cast state but after annealing at 800 °C for 25 h. Further improvements of comprehensive mechanical properties by microstructure tailoring and multiphase engineering are expected in the future.

4 Discussion

The current as-cast WTaHfTiZr RHEA has a dual-phase structure. Due to its metastable structure after solidification in a copper mold, the phase structure could be interpreted by using the empirical criteria, which has been extended from binary dilute alloys to multi-principle alloys [10]. The first

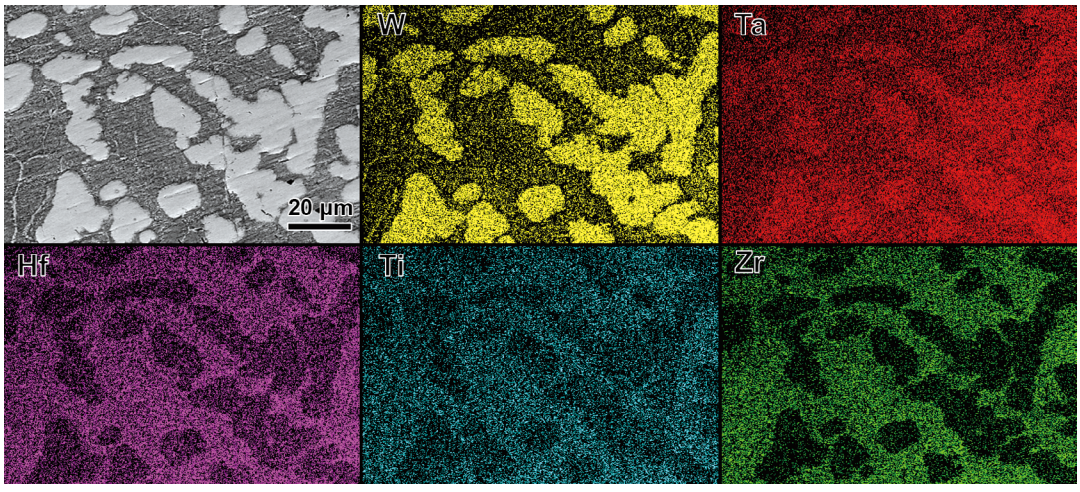

Fig. 3: SEM-EDS maps of as-cast WTaHfTiZr RHEA

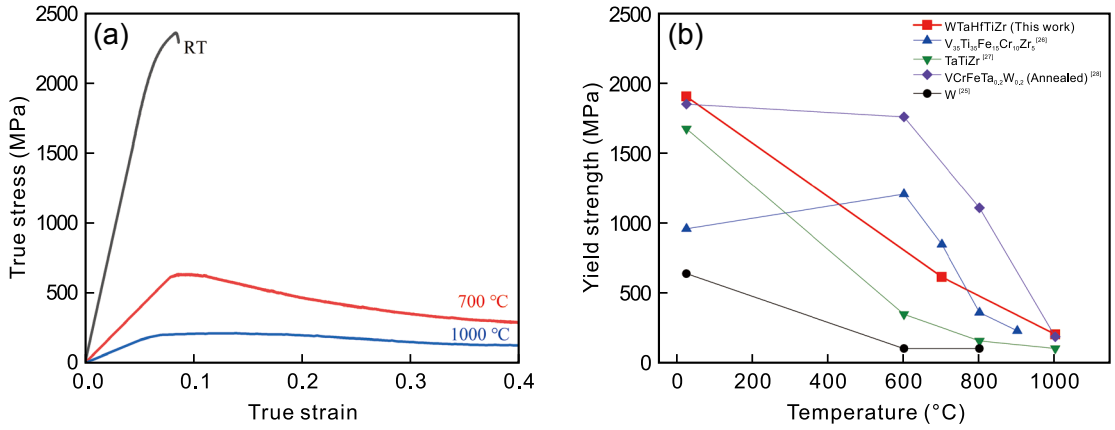

Fig. 4: Compressive true stress-true strain curves of WTaHfTiZr RHEA (a) and comparison of yield strength between WTaHfTiZr RHEA and some low activation alloys (b)

Table 2: Yield strength, compressive strength, and fracture strain of as-cast WTaHfTiZr RHEA deformed at room temperature (RT), 700 °C and 1,000 °C

Temperature (°C)	Yield strength (MPa)	Compressive strength (MPa)	Fracture strain (%)
RT	1,900	2,343	8.1
700	612	630	>40
1,000	203	211	>40

is the modified Hume-Rosery rules with several physical parameters proposed for predicting the phase formation and structural stability in HEAs [10, 29-32], such as T_m (melting point), ΔS_{mix} (mixing entropy), ΔH_{mix} (mixing enthalpy), δ (atomic size difference), Ω (ratio of ΔS_{mix} to ΔH_{mix}) and VEC (valence electron concentration):

$$T_m = \sum_{i=1}^{n} c_i (T_m)_i \quad (2)$$

$$\Delta S_{mix} = -R \sum_{i=1}^{n} c_i \ln c_i \quad (3)$$

$$\Delta H_{mix} = \sum_{i=1, i\neq j}^{n} 4\Delta H_{ij}^{mix} c_i c_i \quad (4)$$

$$\delta = \sqrt{\sum_{i=1}^{n} c_i \left(1 - \frac{r_i}{\bar{r}}\right)^2} \left(\bar{r} = \sum_{i=1}^{n} c_i r_i\right) \quad (5)$$

$$\Omega = \frac{T_m \Delta S_{mix}}{|\Delta H_{mix}|} \quad (6)$$

$$VEC = \sum_{i=1}^{n} c_i (VEC)_i \quad (7)$$

where c_i and $(T_m)_i$ represent the atomic percentage and the melting point of the ith constituent element, respectively. R represents the universal gas constant, and ΔH_{ij}^{mix} represents the mixing enthalpy between the ith and jth component elements. The values of ΔH_{ij}^{mix} are displayed in Fig. 5. The r_i is the atomic radius of the ith component. The number of constituent elements is represented by n. Based on Eqs. (2)–(7) calculation, the obtained T_m, ΔS_{mix}, ΔH_{mix}, δ, Ω and VEC of the WTaHfTiZr RHEA are listed in Table 3.

A previous study [33] suggested that the solid solution phase is formed when $-15<\Delta H_{mix}<5$ kJ·mol^{-1}, $12<\Delta S_{mix}<17.5$ J·K^{-1}·mol^{-1} and $\delta<6.6\%$. Later, Yang et al. [31] introduced a dimensionless parameter Ω to predict the phase formation of HEAs. The conclusion is that a stable solid solution phase can be obtained when $\Omega\geq1.1$. Both parameters of Ω and δ play a vital role in predicting the solid solution formation in HEAs. The greater Ω

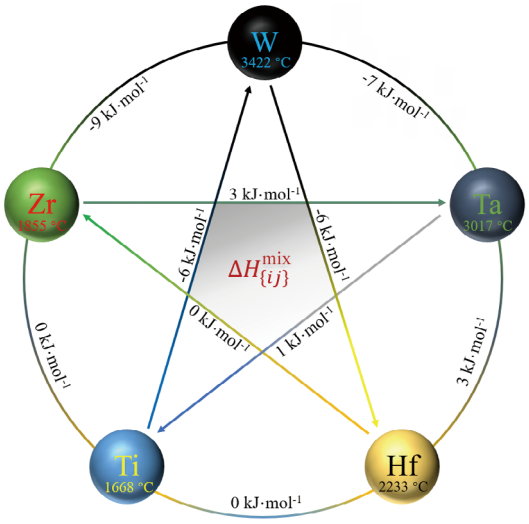

Fig. 5: Mixing enthalpy between any two elements and melting points for each element in WTaHfTiZr RHEA

Table 3: Physical parameters (T_m, ΔS_{mix}, ΔH_{mix}, δ, Ω and VEC) of WTaHfTiZr RHEA

T_m (°C)	ΔS_{mix} (J·K^{-1}·mol^{-1})	ΔH_{mix} (kJ·mol^{-1})	δ	Ω	VEC
2,439	13.38	−3.36	5.9%	10.8	4.6

and smaller δ would promote the formation of a solid solution in HEAs. The above parameters can predict the formation of solid solution, but they cannot distinguish the structure of the solid solution. Therefore, another parameter VEC was proposed [29]. It was described that the stable solid solution phase of FCC should be formed with VEC>8; a single BCC phase is presented when VEC<6.87; and both FCC and BCC phases coexist when 6.87≤VEC≤8.

Based on our calculated data, a stable single BCC solid solution structure should form in the WTaHfTiZr RHEA. However, the experimental results show that the WTaHfTiZr RHEA contains two BCC phases. This phenomenon could be caused by affinities between elements and solute segregation during solidification [32].

In general, the interaction between constituent elements plays a role in phase formation. The interaction between elements could be reflected by mixing enthalpy values. The mixing enthalpies between each element in Fig. 5 indicate that the value between W and Zr is the most negative (-9 kJ·mol^{-1}), and slightly increases to -7 kJ·mol^{-1} between W and Ta and -6 kJ·mol^{-1} between W and Ti/Hf. Ta has positive mixing enthalpies with other elements. However, chemical composition analysis shows that W and Ta, other than Zr or other elements, are enriched both in dendrites and precipitate particles. In practice, the phase formation is determined not only by interaction force but also by the formation conditions. The solidification process of the RHEA from liquid to solid determines its phase constitution by elemental redistribution in local regions, which leads to the different precipitation sequence in liquid for various elements. It can be simply explained by the difference in melting point between elements [28, 34]. Figure 6 is a schematic diagram of the microstructure formation in the WTaHfTiZr RHEA. During solidification, W and Ta with much higher melting points are inclined to solidify preferentially and enriched in the dendrites, while the elements with lower melting points are rejected to the solidification interface. In the last stage of solidification, this behavior also occurs in the interdendritic regions, where the local micro areas rich in W and Ta preferentially solidify. However, they can only grow to fine granular particles since the lower temperature; at this time, the adjacent areas rich in Ti, Zr and Hf reach the solidifying point as well, and begin to solidify. The enrichment of high melting point elements in dendrites and low melting point elements in interdendrites are revealed in the classical CrMnFeCoNi HEA [35].

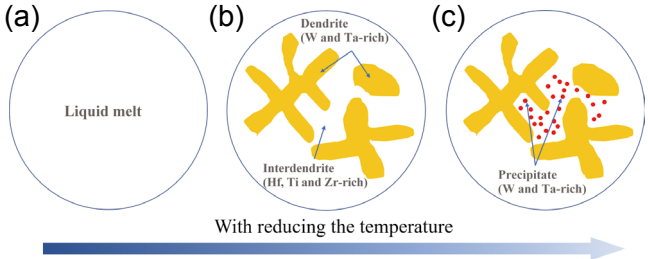

Fig. 6: Schematic diagram of microstructure formation during solidification of WTaHfTiZr RHEA

The WTaHfTiZr RHEA shows high strengths both at room and high temperatures. The high strengths are attributed mainly to solid solution strengthening and second phase strengthening that are available in this composition and microstructure. Different sizes and properties of constituent elements play a role in solid solution strengthening. Then, the dual-phase BCC structure induces the formation of phase boundaries, which can act as obstacles to dislocation movement, thus strengthening the alloy. Researchers also found a similar result in other HEAs. For example, adding W or Mo and W into the HfNbTaTiZr RHEA, the crystal structure changes from single BCC of HfNbTaTiZr to dual-phase BCC of HfNbTaTiZrW and HfNbTaTiZrMoW, and the yield strength increases [14]. A similar example is phase structure evolution of the AlNbTaTiVZr RHEA with Zr, Al and Ti addition, leading to a much higher yield strength of the dual BCC alloy than that of the single BCC alloy [36]. Furthermore, there are a large number of precipitate particles in the WTaHfTiZr RHEA, which hinder the dislocation movement and increase the strength. At elevated temperatures, the RHEA reaches the maximum strength in the deformation process followed by strain softening occurrence. The high-temperature deformation behavior can be explained by work hardening and dynamic softening [16]. However, the deformation mechanism at elevated temperatures of this RHEA has not been well understood, so it needs to be further studied.

5 Conclusions

A novel low activation cast WTaHfTiZr RHEA was prepared. The phase constitution, microstructure and mechanical properties were studied. The obtained results can be summarized as follows:

(1) The as-cast WTaHfTiZr RHEA consists of a dendritic structure with two BCC phases. The dendrite BCC phase is rich in elements with higher melting points (W and Ta), whereas the interdendrite BCC phase is rich in elements with lower melting points (Hf, Ti and Zr).

(2) At room temperature, the alloy has high compressive yield strength of 1,900 MPa and fracture strain of 8.1%, and at elevated temperatures, it still has high compressive yield strength (612 MPa at 700 °C and 203 MPa at 1,000 °C).

(3) The dual-phase BCC structure is caused by the preferential nucleation of W and Ta with much higher melting points during solidification. The high strengths are attributed mainly to solid solution strengthening and second phase strengthening.

Acknowledgements

This work was financially supported by the National Natural Science Foundation of China (Grant Nos. 51971099 and 52071088).

References

[1] Huang B, Xiao Y, He B, et al. Effect of potassium doping on the thermal shock behavior of tungsten. International Journal of Refractory Metals and Hard Materials, 2015, 51: 19–24.
[2] Sun Z P, Li X Z, Wang Z M. Microstructure and mechanical properties of low activation Fe-Ti-Cr-V-W multi-principal element alloys. Journal of Nuclear Materials, 2020, 533(5): 152078.
[3] Pillon M, Angelone M, Arpesella C, et al. Comparison between experimental and numerical determination of neutron-induced activation in low-activation materials. Proceedings of SPIE – The International Society for Optical Engineering, 1997, 2867: 582–585.
[4] Zheng W, Yue Y, Arshad K, et al. Effects of tantalum concentration on the microstructures and mechanical properties of tungsten-tantalum alloys. Fusion Engineering & Design, 2017, 125: 496–502.
[5] Riccardi B, Giancarli L, Hasegawa A, et al. Issues and advances in SiC_f/SiC composites development for fusion reactors. Journal of Nuclear Materials, 2004, 329–333: 56–65.
[6] Wurster S, Baluc N, Battabyal M, et al. Recent progress in R&D on tungsten alloys for divertor structural and plasma facing materials. Journal of Nuclear Materials, 2013, 442(1–3): S181–S189.
[7] Chakin V, Reimann J, Moeslang A, et al. Thermal conductivity of highly neutron-irradiated beryllium in nuclear fusion reactors. Progress in Nuclear Energy, 2012, 57(6): 2–7.
[8] Scaffidi-Argentina F, Longhurst G R, Shestakov V, et al. Beryllium R&D for fusion applications. Fusion Engineering and Design, 2000, 51: 23–41.
[9] Li Z, Long Y, Li Y, et al. Microstructure and properties of needle punching chopped carbon fiber reinforced carbon and silicon carbide dual matrix composite. Ceramics International, 2016, 42(8): 9527–9537.
[10] Zhang Y, Zuo T T, Tang Z, et al. Microstructures and properties of high-entropy alloys. Progress in Materials Science, 2014, 61: 1–93.
[11] Li T X, Lu Y P, Wang T M, et al. Grouping strategy via d-orbit energy level to design eutectic high-entropy alloys. Applied Physics Letter, 2021, 119(7): 071905.
[12] Senkov O N, Wilks G B, Miracle D B, et al. Refractory high-entropy alloys. Intermetallics, 2010, 18: 1758–1765.
[13] Waseem O A, Ryu H J. Powder metallurgy processing of a W_xTaTiVCr high-entropy alloy and its derivative alloys for fusion material applications. Scientific Reports, 2017, 7(1): 1926.
[14] Wang M, Ma Z L, Xu Z Q, et al. Microstructures and mechanical properties of HfNbTaTiZrW and HfNbTaTiZrMoW refractory high-entropy alloys. Journal of Alloys and Compounds, 2019, 803(30): 778–785.
[15] Guo N N, Wang L, Luo L S, et al. Microstructure and mechanical properties of refractory MoNbHfZrTi high-entropy alloy. Materials & Design, 2015, 81(15): 87–94.
[16] Juan C C, Lin C M, Tsai M H, et al. Enhanced mechanical properties of HfMoTaTiZr and HfMoNbTaTiZr refractory high-entropy alloys. Intermetallics, 2015, 62: 76–83.
[17] Li T X, Miao J W, Lu Y P, et al. Effect of Zr on the as-cast microstructure and mechanical properties of lightweight $Ti_2VNbMoZr_x$ refractory high-entropy alloys. International Journal of Refractory Metals and Hard Materials, 2022, 103: 105762.
[18] Lu C Y, Yang T N, Jin K, et al. Radiation-induced segregation on defect clusters in single-phase concentrated solid-solution alloys. Acta Materialia, 2017, 127: 98–107.
[19] Nagase T, Anada S, Rack P D, et al. MeV electron-irradiation-induced structural change in the bcc phase of Zr-Hf-Nb alloy with an approximately equiatomic ratio. Intermetallics, 2013, 38: 70–79.
[20] Li T X, Lu Y P, Cao Z Q, et al. Opportunity and challenge of refractory high-entropy alloys in the field of reactor structural material. Acta Metallurgica Sinica, 2021, 57(1): 42–54. (In Chinese)
[21] Li T X, Miao J W, Guo E Y, et al. Tungsten-containing high-entropy alloys: A focused review of manufacturing routes, phase selection, mechanical properties, and irradiation resistance properties. Tungsten, 2021, 3: 181–196.
[22] Ayyagari A, Salloom R, Muskeri S, et al. Low activation high entropy alloys for next generation nuclear applications. Materialia, 2018, 4: 99–103.
[23] Sadeghilaridjani M, Ayyagari A, Muskeri S, et al. Ion irradiation response and mechanical behavior of reduced activity high entropy alloy. Journal of Nuclear Materials, 2020, 529: 151955.
[24] Waseem O A, Lee J, Lee H M, et al. The effect of Ti on the sintering and mechanical properties of refractory high-entropy alloy Ti_xWTaVCr fabricated via spark plasma sintering for fusion plasma-facing materials. Materials Chemistry and Physics, 2018, 210: 87–94.
[25] Kim I H, Oh H S, Lee K S, et al. Optimization of conflicting properties via engineering compositional complexity in refractory high entropy alloys. Scripta Materialia, 2021, 199: 113839.
[26] Xian X, Zhong Z H, Zhang B W, et al. A high-entropy $V_{35}Ti_{35}Fe_{15}Cr_{10}Zr_5$ alloy with excellent high-temperature strength. Materials & Design, 2017, 121: 229–236.
[27] Senkov O N, Kuhr S J, Shank J M, et al. Microstructure and properties of an equiatomic TaTiZr alloy. Materials Science and Engineering: A, 2021, 814: 141168.
[28] Zhang W R, Liaw P K, Zhang Y. A novel low-activation $VCrFeTa_xW_x$ (x = 0.1, 0.2, 0.3, 0.4, and 1) high-entropy alloys with excellent heat-softening resistance. Entropy, 2018, 20(12): 951.
[29] Guo S, Ng C, Lu J, et al. Effect of valence electron concentration on stability of fcc or bcc phase in high entropy alloys. Journal of Applied Physics, 2011, 109: 103505.
[30] Sheikh S, Shafeie S, Hu Q, et al. Alloy design for intrinsically ductile refractory high-entropy alloys. Journal of Applied Physics, 2016, 120: 164902.
[31] Yang X, Zhang Y. Prediction of high-entropy stabilized solid-solution in multi-component alloys. Materials Chemistry and Physics, 2012, 132(2–3): 233–238.
[32] Qin G, Chen R R, Liaw P K, et al. An as-cast high-entropy alloy with remarkable mechanical properties strengthened by nanometer precipitates. Nanoscale, 2020, 12: 3965–3976.
[33] Zhang Y, Zhou Y J, Lin J P, et al. Solid-solution phase formation rules for multi-component alloys. Advanced Engineering Materials, 2008, 10: 534–538.
[34] Li T X, Jiao W N, Miao J W, et al. A novel ZrNbMoTaW refractory high-entropy alloy with in-situ forming heterogeneous structure. Materials Science and Engineering: A, 2021, 827: 142061.
[35] Laurent-Brocq M, Akhatova A, Perrière L, et al. Insights into the phase diagram of the CrMnFeCoNi high entropy alloy. Acta Materialia, 2015, 88: 355–365.
[36] Senkov O N, Woodward C, Miracle D B. Microstructure and properties of aluminum-containing refractory high-entropy alloys. JOM, 2014, 66: 2030–2042.